Fatigue properties and characterization of tungsten heavy alloys IT180 & D176

CrossMark

P. Lorenzo [a], M. Miralda [a], S. Iyengar [a,*], S. Melin [b], Etam Noah [c]

[a] Materials Engineering, Lund University, 22100 Lund, Sweden
[b] Mechanics, Lund University, 22100 Lund, Sweden
[c] European Spallation Source Scandinavia, Lund, Sweden

ABSTRACT

Fatigue properties of tungsten heavy alloys IT180 (W-3.5Ni-1.5wt.%Cu) and D176 (W-5Ni-2.5wt.%Fe) have been determined using constant amplitude, stress-controlled high cycle fatigue tests at room temperature. The results show that the endurance limits for the IT180 and D176 alloys are about 210 and 425 MPa respectively. The fatigue strength coefficients for the two alloys have been determined as 1048 and 3000 MPa and the corresponding strength exponents are -0.11 and -0.13 respectively. Strain-controlled fatigue tests were also performed to observe the response of the materials and determine the cyclic stress–strain curves of the alloys using the multiple step method. Cyclic hardening was observed in both alloys and the cyclic strain hardening exponent for the D176 alloy had a value of 0.08. The fatigue response of the material is strongly affected by surface roughness, residual porosity, pore size and its distribution. Microstructures and the fracture surfaces of the samples were characterized by scanning electron microscopy and energy dispersive spectroscopy.

© 2013 Elsevier Ltd. All rights reserved.

1. Introduction

European Spallation Source (ESS) is a joint European project to build a large-scale research facility to produce neutrons for materials characterization through scattering experiments. In the spallation process, neutrons are produced by bombarding a target with high-energy protons. Currently the ESS is in the pre-construction phase and a decision has been taken to use tungsten as the target material after investigating other potential target materials including tungsten heavy alloys. High power targets have to withstand a large average beam power varying in space and time which induces a combined load of high radiation damage and large temperature gradients, leading to cyclic thermal stresses in the target material. This study deals with the determination of fatigue properties of some tungsten heavy alloys at room temperature.

2. Materials and methods

In the present work, mechanical properties (tensile and fatigue) of two different tungsten heavy alloys, IT180 (W-3.5Ni-1.5wt.%Cu) and D176 (W-5Ni-2.5wt.%Fe) have been determined at room temperature, after microstructural characterization of the alloys. These powder metallurgical products were supplied by Plansee and were presumably liquid-phase sintered. For purposes of testing, 13 specimens of IT180 and 10 specimens of D176 were used in this study. The specimen geometry is shown in Fig. 1.

The specimens presented considerable surface roughness in the as-received condition and were ground using silicon carbide papers in the sequence 320, 500, 1000 and 4000 particles per square inch, followed by polishing with 3 μm and 1 μm diamond suspensions. The average specimen diameter after the polishing treatment was 4.99 ± 0.01 mm. The specimens were stored in a desiccator prior to testing.

The mechanical testing was performed at room temperature in a MTS Ramen machine controlled by a Digital Electronic system (Instron). Tensile testing was performed at a constant displacement rate of 0.05 mm/s. At a frequency of 30 Hz, stress controlled fatigue testing under fully reversed loading conditions (i.e. stress ratio $R_\sigma = -1$) was carried out to obtain median Wöhler S–N curves and design curves within the relatively high cycle fatigue region $10^4 < N < 10^6$, with N denoting the number of cycles to failure. The curves were obtained using applied statistical methods suggested in the ASTM standard practice E739 [1]. IT180 specimens were tested in the stress interval 200 to 300 MPa, while the D176 specimens were subjected to stresses in the interval 300 to 550 MPa. A minimum of two tests were performed at each stress level.

Strain controlled fatigue testing was also performed to obtain the cyclic stress–strain curves and determine the degree of hardening of the materials. The curves were obtained by testing a solitary specimen of each alloy using the Multiple Step Test method (MST) [2,3] at a strain ratio (R_ε) of -1 and a constant displacement rate of 0.05 mm/s. This was obtained by varying the frequency in each block of successively increasing constant total strain amplitude. For the IT180 alloy, the strain amplitudes used were 0.1 and 0.2%. For the D176 alloy, an amplitude sequence between 0.2 and 1%, in steps of 0.1%, was used.

* Corresponding author. Tel.: +46 462227984.
E-mail address: srinivasan.iyengar@material.lth.se (S. Iyengar).
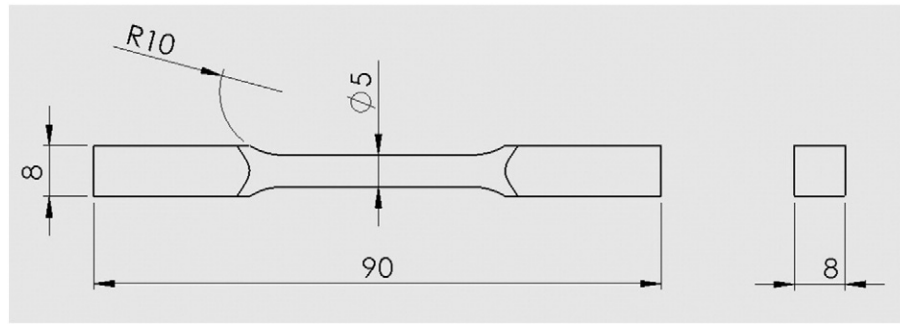
Fig. 1. Specimen geometry (dimensions in mm).

In order to get an idea about the porosities in the samples, densities of the alloy specimens were determined using the Archimedes principle. An attempt was also made to characterize the distribution of porosity along the axial direction in the specimens using recommended procedures [4,5]. This was done with a view to relate crack initiation sites to porosity content in the specimens.

The microstructures of the alloys were examined using optical and Scanning Electron Microscopy (SEM). The phase compositions were determined using Energy Dispersive Spectroscopy (EDS).

3. Results and discussion

3.1. Mechanical properties

3.1.1. Tensile testing

Each alloy (one specimen) was tested in tension according to ASTM practice E8 [6] and the stress–strain curves obtained are shown in Figs. 2

Fig. 2. Stress–strain diagram for IT180 alloy.
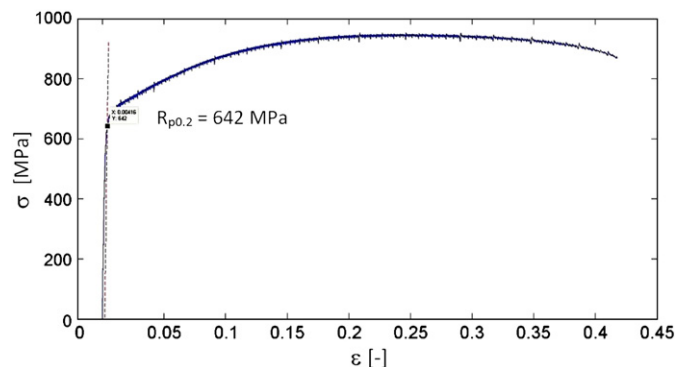
Fig. 3. Stress–strain diagram for D176 alloy.

and 3. Data on the yield strength ($R_{p0.2}$), ultimate tensile strength (R_m), fracture strain (ε_f) and the Young's modulus (E) are summarized in Table 1. For purposes of comparison, data provided by Plansee are also included in the table. The differences observed between the results obtained in the present study and those provided by Plansee could be due to variations in porosity levels and the extent of cold work in the specimens tested. It is also seen that the yield strengths as well as the Young's moduli do not vary much between the alloys. Unlike the elastic properties, there are significant differences in the ultimate tensile strengths and ductilities of the two alloys. This is primarily due to the higher amount of tungsten contained in IT180.

3.1.2. Stress-controlled fatigue experiments

Fatigue experiments were carried out under stress control using 11 specimens of IT180 and 8 specimens of D176. In these experiments, the procedure recommended by ASTM practice E466 [7] was followed. The first test was carried out at a stress level of 50% of the ultimate tensile strength and the following stress levels were chosen either higher or lower than this value depending on whether the specimen had failed or not. As the focus in the present study was on a fatigue life in the interval 10^4 to 10^6 cycles, a specimen enduring 2×10^6 cycles was considered a run-out and the test was interrupted. For other stress levels at which the specimens failed, a minimum of two tests were performed.
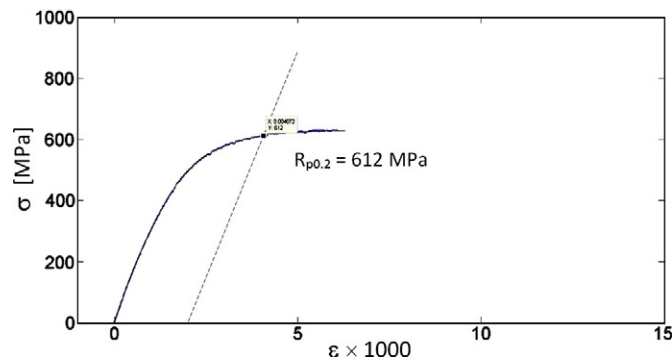
Table 1
Tensile properties of IT180 and D176 alloys.

Mechanical property	IT180		D176	
	Present work	Plansee	Present work	Plansee
$R_{p0.2}$ [MPa]	612	610	642	620
R_m [MPa]	631	685	945	880
ε_f [%]	0.6	3	42	20
E [GPa]	308	360	309	360

Table 2
Stress-controlled fatigue data for IT180 alloy.

Specimen #	σ_a [MPa]	d [mm]	N [cycles]
3	300	4.99	33,831
4	300	4.99	40,177
5	200	4.98	[a]6×10^6
6	200	4.98	2×10^6
7	250	4.98	139,854
8	225	4,98	336,042
9	210	4.99	312,378
10	210	4.99	2×10^6
11	210	4.99	1.63×10^6
12	250	5.00	329,748
13	225	5.00	424,545

[a] Experiment was continued up to this limit (only for #5).

Table 3
Stress controlled fatigue data for D176 alloy.

Specimen #	σ_a [MPa]	d [mm]	N [cycles]
3	300	5.00	2×10^6
4	400	4.99	2×10^6
5	500	4.99	958,423
6	450	4.99	885,444
7	550	4.99	213,838
8	450	4.99	1.47×10^6
9	550	4.99	258,788
10	500	4.99	629,575

Table 4
Median and design curve parameters for IT180 and D176 alloys.

Parameters	IT180	D176
σ'_f [MPa]	1048	3000
b [−]	−0.112	−0.128
σ'_{fLB} [MPa]	868	2553
σ_{fT} [MPa]	633	1180

The experimental results are presented in Tables 2 and 3. σ_a denotes the applied stress amplitude, d is the specimen diameter and N represents either the number of cycles to failure or run-out (2×10^6).

To construct a median S–N curve based on statistical analysis in the interval $10^4 < N < 10^6$, the materials were assumed to follow a Basquin type relationship according to

$$\sigma_a = \sigma'_f (2N)^b \tag{1}$$

where σ'_f is the fatigue strength coefficient and b is the fatigue strength exponent. These parameters can be obtained from the median curve by statistical analysis according to the procedure outlined in the standard ASTM practice E739 [1]. For IT180, four stress levels (300, 250, 225 and 210 MPa) with a total of 9 specimens (excluding specimens #5 and #6) were used for the calculations, with a replication percentage of 55.6%. It should be noticed that E739 pre-supposes that there are no run-outs or suspended tests within the test interval. However,

Specimen #10 of IT180 was actually a run-out that had not failed even after $2\,10^6$ cycles. Nevertheless, it was decided to include this specimen in the calculations since two other specimens actually failed before run-out at the same stress level.

In the case of D176, three stress levels, (550, 500 and 450 MPa), were used with a total of 6 specimens (excluding specimens #3 and #4) giving a 50% replication.

In both cases, the minimum number of specimens and the percentage of replication are in accordance with the requirements of E739 when performing preliminary and exploratory research.

In order to obtain a design curve, the choice was set on a linear, one-sided lower bound estimate. It may be noted that ASTM E739 [1] suggests the use of double-sided hyperbolic confidence intervals. However, this practice also agrees on the use of a linear, one-sided lower bound as a confidence band. In this connection, it was decided to use the commonly accepted approach of the Approximate Owen Tolerance Limit [8–10], using a reliability of 90% with 95% confidence (R90C95). Using this method, the median curve $Y = \overline{A} + \overline{B}X$, with estimators $\overline{A}$ and $\overline{B}$ and variance σ_0, can be shifted to the position $Y = \overline{A} + \overline{B}X - K_{OWEN} \cdot \sigma_0$ on a log–log scale, giving the Basquin relation

$$\sigma_{aLB} = \sigma'_{fLB} (2N)^b \tag{2}$$

where the suffix *LB* refers to the lower bound. Table 4 summarizes the parameters corresponding to the Basquin relations (1) and (2). Also given in the table is the true fracture strength (σ_{fT}) from the monotonic tensile test, compensated for necking. Figs. 4 and 5 show the experimental data from the stress-controlled fatigue experiments together with the statistical median curve and the lower bound Owen estimate with 90% reliability and 95% confidence.

A comparison of data for IT180 and D176 shows that D176 has higher fatigue strength, enduring a larger number of stress reversals as compared to IT180 at similar stress levels. The endurance limit for D176 is about 45% of its ultimate tensile strength and the corresponding value for IT180 is about 33% (Table 1). This is on the lower side of typical endurance limit values for most metals [11].

The values of the stress exponent for most metals have been reported [11] to be between −0.05 and −0.12 which is in agreement with the values obtained for the alloys studied in this work. It is suggested [11] that for most metals, the parameter σ'_f can be approximated
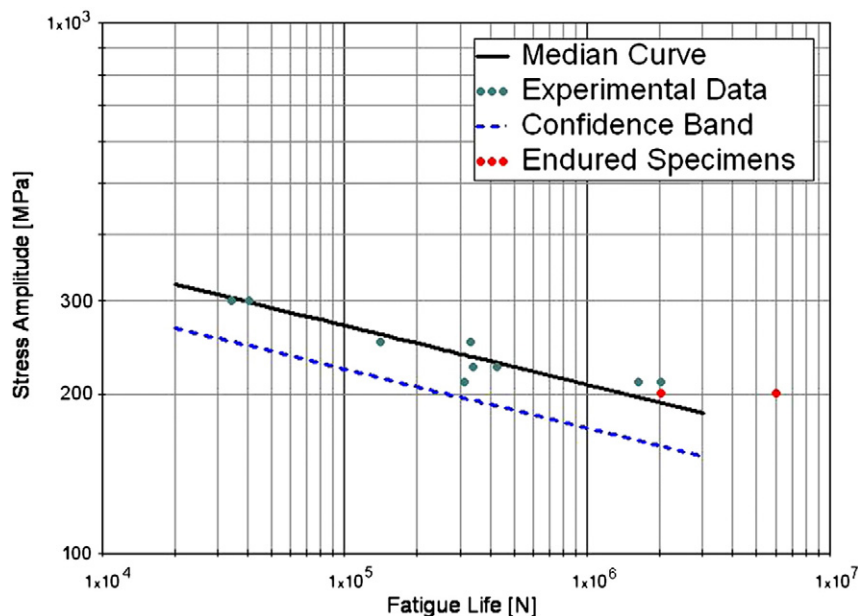

Fig. 4. Experimental data for the IT180 alloy in the finite life region. (— Statistical median curve; ------ lower Owen confidence band).
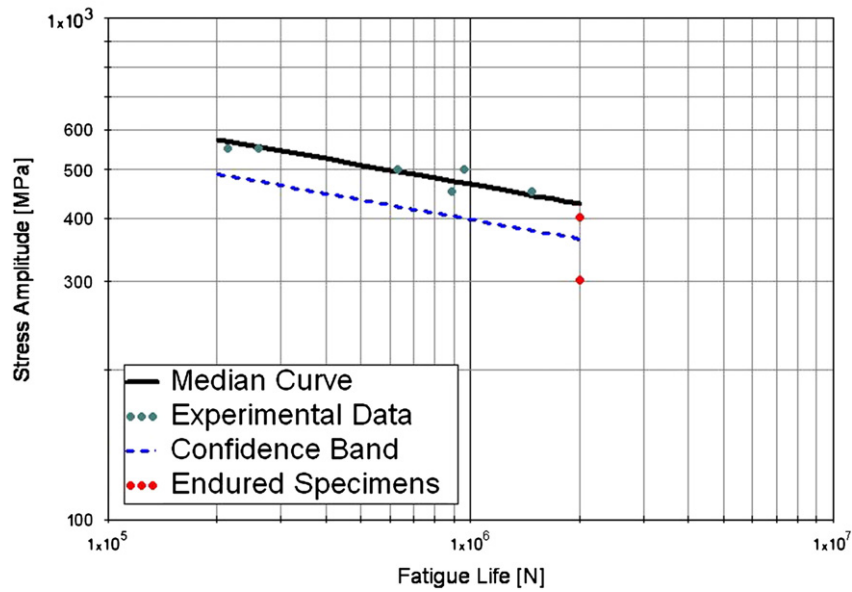
Fig. 5. Experimental data for the D176 alloy in the finite life region. (— Statistical median curve; ------ lower Owen confidence band).

by the true fracture strength σ_{fT}, after correction for necking in a monotonic tensile test. This value would correspond to the intercept on the ordinate in the S–N plot, at one-quarter of the first cycle. In the present case, the true fracture strengths for the IT180 and D176 are estimated as 633 MPa and 1180 MPa while the corresponding fatigue strength coefficients for the alloys are estimated as 1048 MPa and 3000 MPa respectively (Table 4). Keeping in mind that the actual S–N curve is approximated by a linear relationship within a limited range and that the actual fatigue life distribution is unknown, extrapolation of the S–N curve outside the test interval is not recommended. Further, the difference between the true fatigue strength σ_{fT} and the calculated values of σ'_f (particularly for D176) suggest that the median curve should not be extrapolated to the low cycle region. The comparison between σ'_f and σ_{fT} is approximate and it does not necessarily follow that these stresses have to be equal.

3.1.3. Strain-controlled fatigue experiments

To explore the hardening behavior of the alloys, strain controlled experiments were carried out using the method of MTS [2,3,12]. Specimen #2 was used for these tests and the procedure outlined in the ASTM standard E606 [13] was followed. Assuming a Ramberg–Osgood material behavior, the cyclic stress strain curve is expressed as [11]:

$$\varepsilon_a = \frac{\sigma_a}{E} + \left(\frac{\sigma_a}{K'}\right)^{1/n'} \tag{3}$$

where ε_a is the strain amplitude, K' is the cyclic strength coefficient and n' is the cyclic strain hardening exponent.

Alloy IT180 was tested at a strain ratio $R_\varepsilon = -1$, using blocks with two strain amplitudes (ε_a) of 0.1 and 0.2%. The material showed almost elastic behavior at a strain amplitude of 0.1%. Increasing this value to 0.2% led to the stabilization of the loop after 15 cycles at a peak tensile stress of 519 MPa. The specimen failed at this strain level in the 29th cycle.

The first quadrant of the hysteresis loops together with superimposed tensile data is shown in Fig. 6 for the IT180 alloy. The cyclic parameters K' and n' were not estimated due to difficulties in obtaining a sufficient number of data points for this brittle alloy. However, it is observed that the cyclic curves lie above the monotonic curve even in the elastic region and it is apparent that IT180 hardens under cyclic loading.

In the case of D176 alloy, the specimen was loaded by strain blocks in the interval 0.2 to 1%, in steps of 0.1% and with a strain ratio of $R_\varepsilon = -1$. The first quadrant of the hysteresis loops together with superimposed tensile data is shown in Fig. 7. For initial strain amplitudes between 0.2 and 0.5%, the cyclic hardening rate is more noticeable and the loop stabilizes around the 20th cycle of each block. At higher strain amplitudes, the variation of stress amplitude between cycles is small and stabilized hysteresis loops are obtained after only a few cycles.
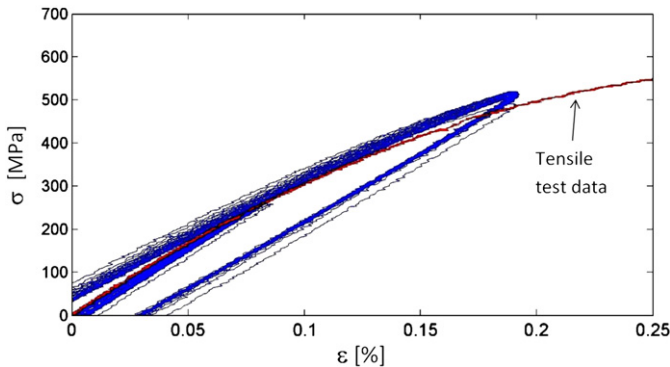

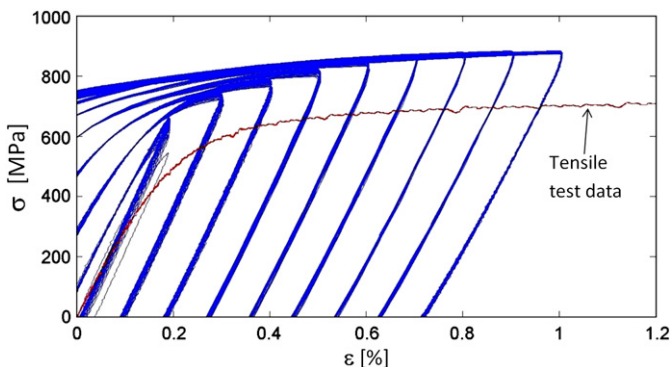**Fig. 6.** Hysteresis loops and tensile data for the IT180 alloy.

Fig. 7. Hysteresis loops and tensile data for the D176 alloy.

Table 5
Densities and porosities of IT180 and D176 alloys.

Alloy	Density Present work g/cm^3	Density By Plansee g/cm^3	Porosity [%]
IT180	18.05	18.0	0.782
D176	17.56	17.6	0.188

The cyclic material parameters K' and n' can be estimated from the plastic stress–strain amplitude data according to the following equation [1]:

$$\sigma_a = K'\left(\varepsilon_p\right)^{n'}; \varepsilon_p = \varepsilon_a - \frac{\sigma_a}{E} \tag{4}$$

where ε_p is the plastic strain amplitude. The monotonic strength coefficient K and the monotonic strength exponent n_m for the tensile curve can be estimated in the same manner as for the cyclic parameters [16].

For the D176 alloy, the cyclic parameters K' and n' were found to be 1314 MPa and 0.08 respectively. The corresponding monotonic parameters K and n_m were determined to be 1008 MPa and 0.07 respectively.

The cyclic yield stress $R'_{p0.2}$ at 0.2% plastic strain on a cyclic stress–strain diagram was determined as suggested by Woodward and O'Donnell [15]. The cyclic yield strength ($R'_{p0.2}$) of the D176 alloy was found to be about 800 MPa, which is higher than the monotonic yield strength ($R_{p0.2}$) which is about 654 MPa (Table 1). This shows the degree of hardening of D176 under cyclic loading, despite the small difference between the cyclic and monotonic strain hardening exponents.

3.2. Materials characterization

3.2.1. Density determination

Densities of both the alloys were determined experimentally using the Archimedes principle and percentage of porosity was then calculated. The results obtained and the values provided by Plansee are shown in Table 5. In these measurements, three specimens were used for each alloy, with the samples taken from the grip regions of stress-fatigued specimens. Microscopic studies also confirmed that IT180 had a higher porosity than D176.

3.2.2. Surface examination

The presence of some pores in powder metallurgical products is unavoidable and it is difficult to attain theoretical density even after proper sintering. Examination of the current specimens using optical microscopy showed the presence of a large number of pores of varying shapes and sizes. These could affect the fatigue response of the material by acting as crack initiation sites. According to Chawla et al. [14,16], crack initiation in sintered powder compacts is sensitive
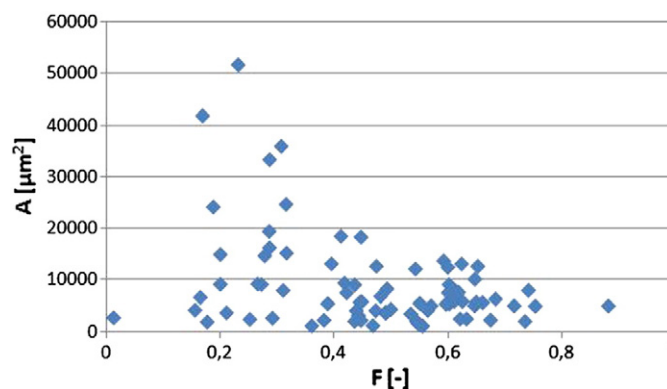
Fig. 9. Form factor calculated for all the pores observed in three IT180 specimens.

to the size and shape of the pores. Large pores which have an irregular shape are more detrimental from a fatigue point of view. It is therefore highly relevant to localize large pores on the specimen surface to see to what extent large pores are present in the area of failure. The largest pore observed in an IT180 specimen in the as received condition had a diameter of 280 μm. In this work, pores with at least one linear measure larger than 100 μm have been considered to be of interest.

Optical images showing the pores and roughness on an IT180 specimen surface in the as-received condition and after grinding and polishing are presented in Fig. 8. Both the images refer to the same area of the specimen and it may be noted that surface treatment, besides reducing the roughness, can remove small pores, but can also reveal new pores which were not visible earlier.

A form factor F, suggested previously by Chawla et al. [14,16], was used to characterize the irregularities of the surface pores. It is defined as:

$$F = \frac{4\pi A}{P^2} \tag{5}$$

where A is the pore area and P is the pore perimeter. Values of F close to unity represent nearly spherical pores while values close to zero indicate a completely irregular pore. Fig. 9 shows all the shape factors found from an inspection of the entire measuring lengths of three different specimens of IT180 before testing. It is seen that the larger pores have a lower form factor whereas the smaller ones have a higher form factor indicating a more regular and near spherical shape of small pores.

It was further observed that the pores were not uniformly distributed along the specimen. While the crack initiation in powder metallurgical materials is associated with the size and shape of the pores, the mean pore spacing is a factor that affects the crack propagation
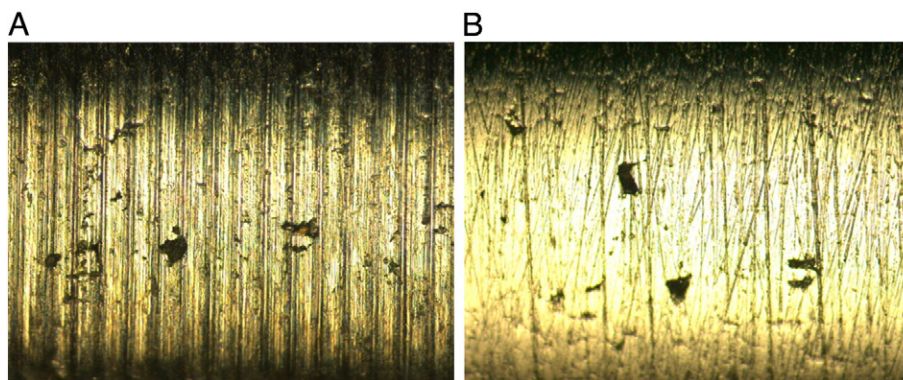
Fig. 8. Porosity and roughness on the specimen surface (100×). (A) in as-received condition and (B) after grinding and polishing.
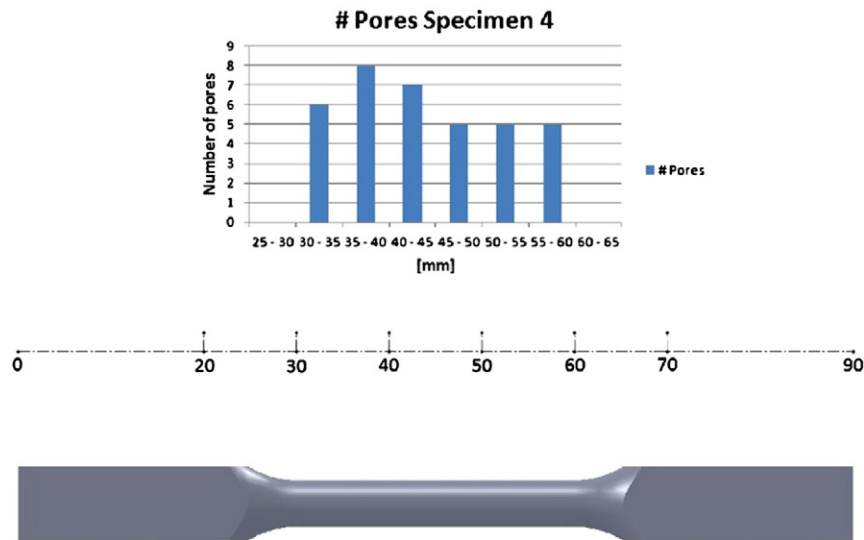
Fig. 10. Pore distribution along specimen #4, IT180. Fracture at 38 mm.
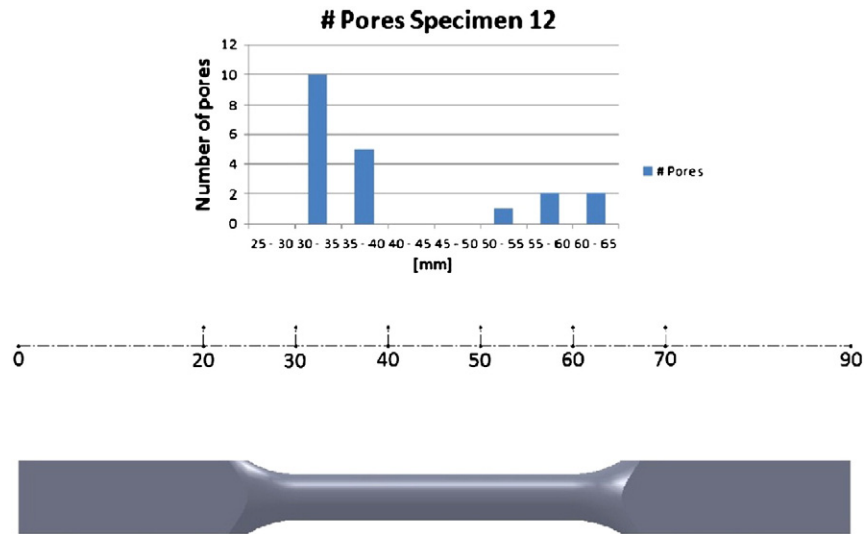

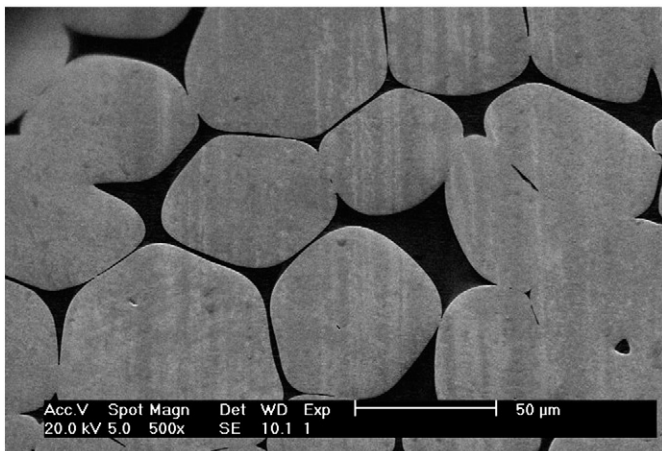**Fig. 11.** Pore distribution along specimen #12, IT180. Fracture at 60 mm.

Fig. 12. Microstructure of IT180 alloy.

rate. When pores are evenly distributed and closely spaced, the crack propagates only a short distance before encountering the next pore, which instantly increases the crack length. However, in materials with high density but with a small amount of porosity, the presence of pores might actually reduce the speed of crack growth by providing a braking effect and introducing a deviation to the path of crack propagation.

As a general observation, more zones with clusters of pores were found in IT180 specimens as compared to relatively widely spaced and isolated pores in D176.

Eight specimens of IT180 with higher porosity were closely examined for locating pores in the fracture area. In five of them, fracture took place in a zone of significantly higher pore concentration. In two specimens, the porosity was not significantly high in the region where fracture occurred. In one of the specimens, the bigger pores were not located near the fracture area. In general, crack initiation appears to be more likely in areas of high porosity.

Some specimens failed near the neck area, but still within the gauge length. In order to investigate the correlation between failure
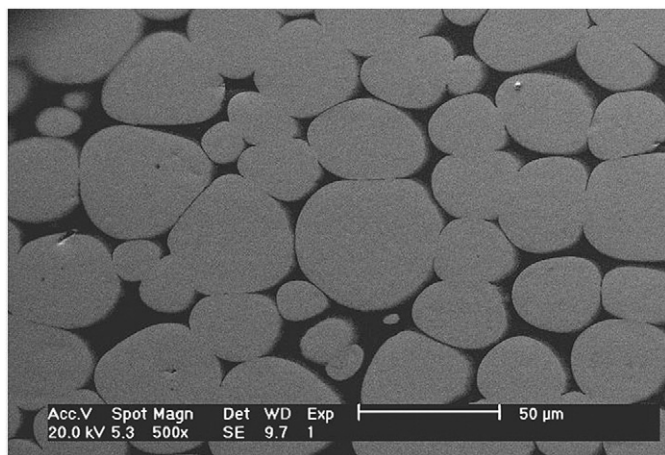
Fig. 13. Microstructure of D176 alloy.

and pore density, eight IT180 specimens were scanned along the axial direction to count the number pores with at least one linear dimension larger than 100 μm. Figs. 10 and 11 show the results obtained for two specimens. In general, a large amount of pores are present close to the neck region and the blend radius acts as a stress concentrator and finite element calculations show a stress concentration factor slightly above unity ($K_t = 1.03$).

3.2.3. Microstructure

Fig. 12 shows the microstructure of IT180 alloy as observed in the scanning electron microscope. The microstructure is characterized by the presence of tungsten grains with an average diameter of 62 μm and a bonding phase in between the grains. In a similar study, Dasa

et al. [17] reported the tungsten grain diameter to be about 60 μm. The image also shows that the tungsten–tungsten interfacial area is significant and that most of the pores are present at the grain boundaries.

Fig. 13 shows the microstructure of D176 observed in the SEM. The average tungsten grain size in this alloy is 34 μm. This alloy has more rounded pores and the tungsten grains are relatively much smaller than those in IT180. In general, tungsten alloys containing nickel and iron have smaller tungsten grains and fewer tungsten–tungsten interfacial areas relative to those containing nickel and copper.

The tungsten content is one of the main factors responsible for the differences in microstructure and mechanical properties between tungsten heavy alloys. Higher tungsten contents require higher sintering temperatures that inevitably results in larger grains [17]. Increasing the amount of tungsten decreases the amount of binder phase and, consequently, the tungsten–matrix interface area [18]. This results in a larger tungsten–tungsten interfacial area. This last feature, also known as contiguity, characterizes the amount of tungsten–tungsten interface area in proportion to the total interface area and is an important feature that affects the ductility of these alloys. In the present case, the higher amount of tungsten is responsible for the lower ductility of the IT180 alloy. Fracture toughness data for some tungsten heavy alloys have been reported by Zamora et al. [19].

X-ray mapping of the specimen surfaces, seen in Figs. 14 and 15, showed that the grains correspond to almost pure tungsten while the alloying elements are distributed in the binder phase. From a quantitative point of view, analyses of both alloys (Table 6) show that the binder phase of D176 is richer in tungsten (~50 wt.%) as compared to that of IT180 (~30 wt.%). Fig. 16 shows the results of spot analyses in the matrixes (ductile phases) of both alloys. Furthermore, in the case of D176 the amount of nickel is very low as compared to the amount of iron. It is also worth noticing the high percentage of tungsten in the ductile phase of D176.
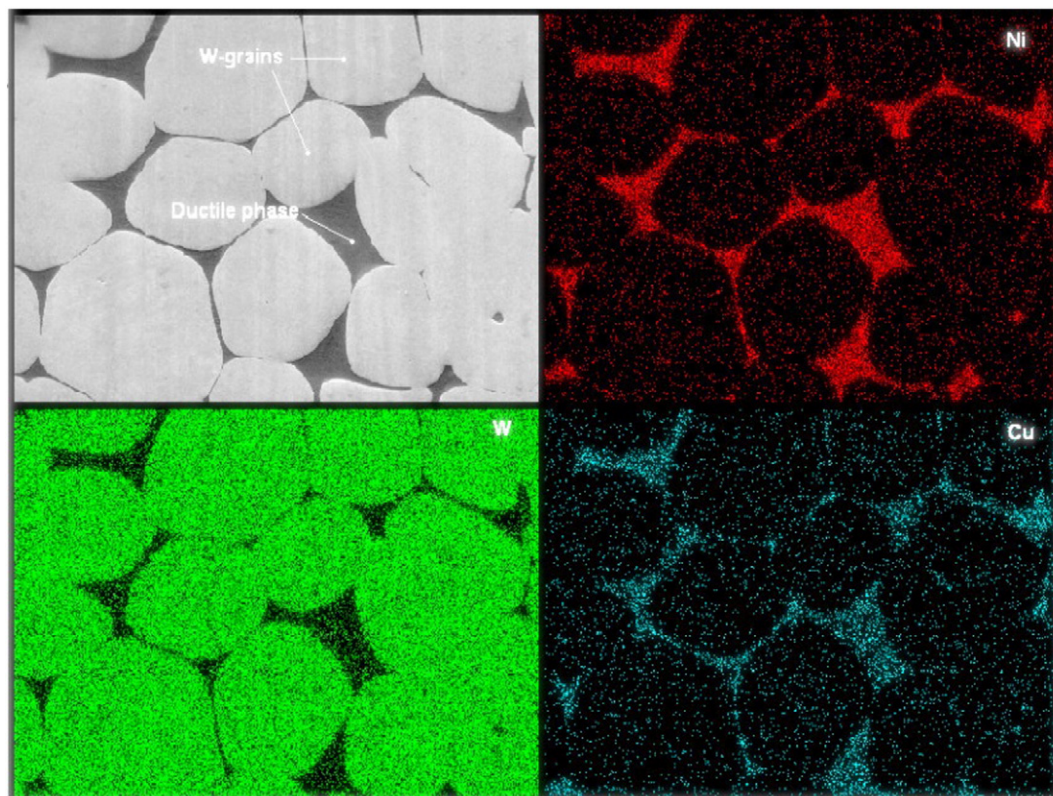

Fig. 14. X-ray maps showing the distribution of nickel, tungsten and copper (IT180 alloy).
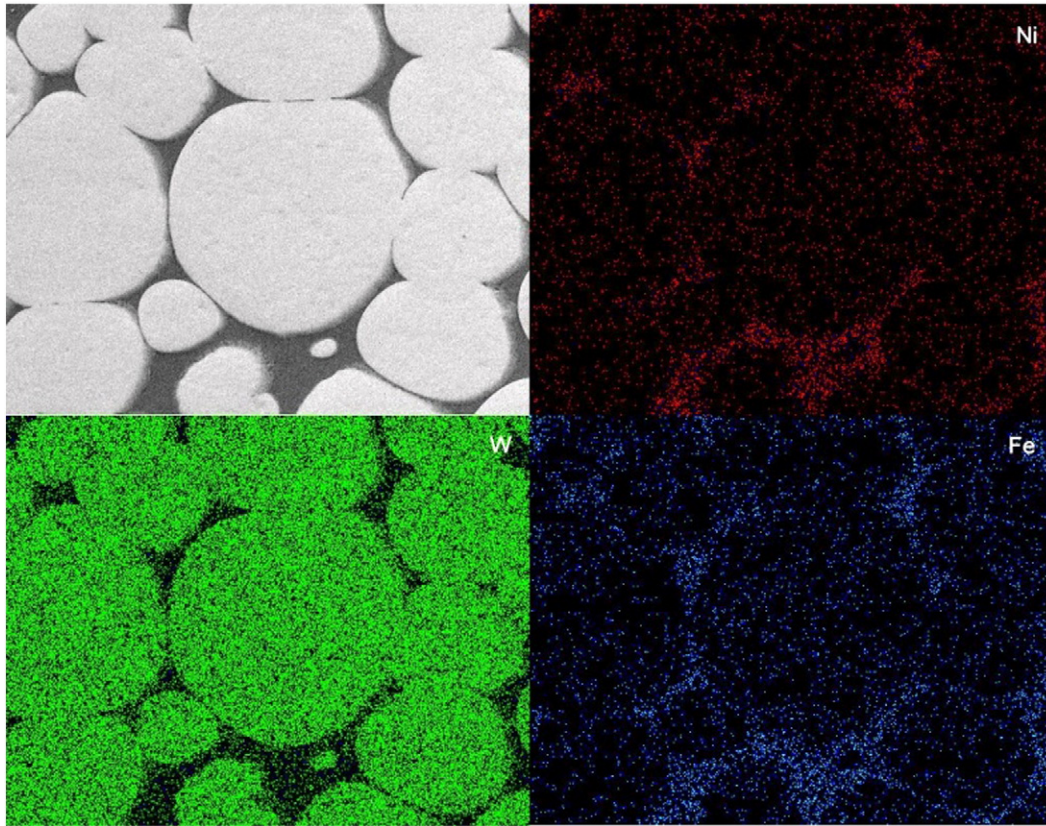
Fig. 15. X-ray maps showing the distribution of nickel, tungsten and iron (D176 alloy).

3.2.4. Fractographic studies

Fig. 17A shows the fracture surface after stress controlled fatigue fracture of an IT180 alloy specimen. Failure at the tungsten–matrix interface as well as decohesion at the tungsten–tungsten interface can be observed. This alloy of relatively higher tungsten content and lower ductility is characterized by a large interfacial area between the tungsten grains. Decohesion at such interfaces plays a dominant role in the fracture of these specimens.

In the case of D176, a combination of tungsten–matrix failure and transgranular cleavage of tungsten grains can be observed in Fig. 17B, showing a specimen that fractured under stress control. The figure shows how the cracks propagate between the grain boundaries and the ductile matrix, and then through the grains giving them the observed radial striations. Evidence of intergranular failure to a minor extent is also seen in the figure.

Tungsten–tungsten interfaces are weak links in the microstructure and the easiest path for crack growth. The critical energy release rate is the lowest for decohesion of these interfaces [13,15]. Alloys with high contiguity have a lower ductility because they have a large amount of low strength bonds between tungsten grains that can fail easily under minor loads.

4. Conclusions

The S–N curves of the alloys show that Densimet 176 has a higher fatigue strength than Inermet 180. Corresponding endurance limits have been estimated to be about 45% and 33% of the ultimate tensile strengths for the alloys, respectively.

The tungsten content affects the fatigue behavior of these alloys. The higher the tungsten content, the lower the fatigue properties which explains why D176 (92.5 wt.% W) has a higher fatigue strength than IT180 (95 wt.% W).

Porosity is a common defect present in both alloys. However its effect has been more detrimental in the case of IT180 which presented bigger pores, with a very irregular shape and in large amounts that led to stress concentrations and zones of crack initiation. The scatter in the fatigue data for this alloy is higher than that of D176 and might be related to this fact.

The use of stress-controlled testing for estimating the Wöhler S–N curve is fairly valid since all the specimens endured more than 10^4 cycles before failing, proving that the experiments were in the high cycle fatigue regime where this type of test is suitable.

Since the Wöhler relationship was approximated by a straight line within the tested stress interval and the actual fatigue distribution is unknown, the results obtained should not be extrapolated to other stress levels and are only valid within this interval.

Surface roughness has a detrimental effect on crack initiation in a material under cyclic loading. Grinding and polishing to reduce radial lines on the surface of the specimens decreased this effect and improved the reproducibility of the fatigue results. The stress concentration factor associated with the blend radius of the tested specimens has a bearing on the failure of the specimens near the grips. More accurate results can be obtained bby testing samples with the same shape as the target material envisaged for use in the spallation source. The

Table 6
Spot analysis showing the ductile phase composition in the alloys (wt.%).

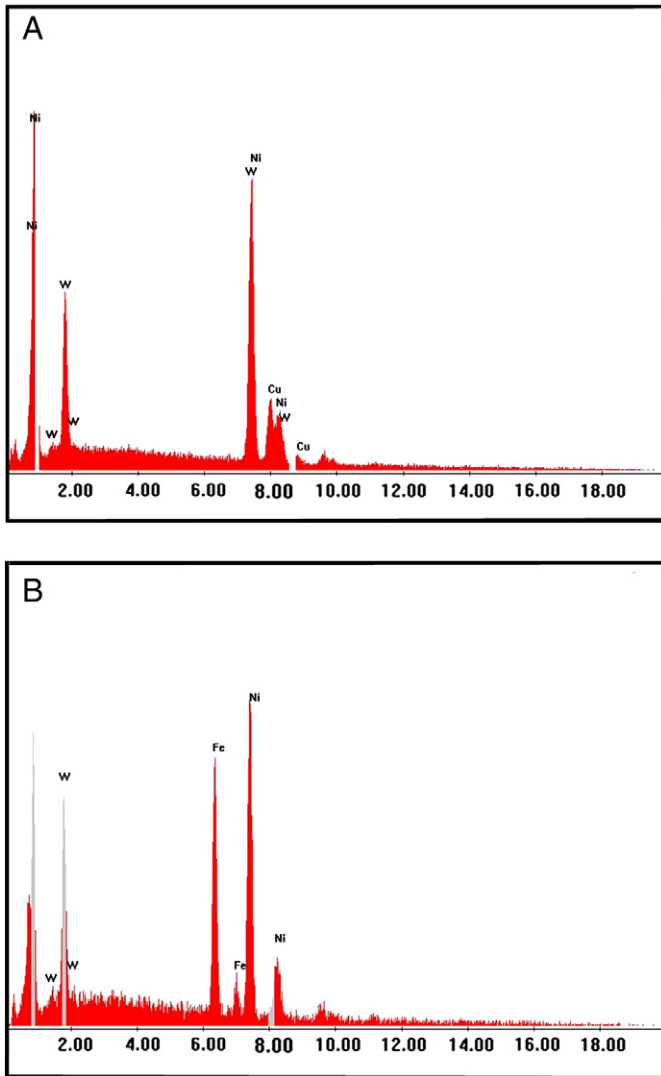| Alloy	W	Ni	Cu	Fe
IT180	33.34	47.12	19.54	
IT180	30.66	50.77	18.57	
D176	51.38	16.39		32.23
D176	50.77	17.32		31.91

Fig. 16. EDS spectra for the ductile phase in (A) IT180 and (B) D176 alloys.

principal fracture mechanism under fatigue loading observed in D176 was tungsten grain cleavage while in the case of IT180, intergranular failure by separation of W–W interfaces was predominant.

The cyclic stress–strain curves showed that both alloys harden under cyclic loading as compared to their response under tensile loads. The cyclic strain hardening exponent and the yield strength of D176 determined from the experimental data are higher than the monotonic strain hardening exponent and yield strength. It was not possible to determine these parameters for the brittle IT180 alloy which failed at low strain levels.

Acknowledgments

References

[1] American Society for Testing Materials. Standard Practice for Statistical Analysis of Linear or Linearized Stress-Life (S-N) and Strain-Life (e-N) Fatigue Data, E739; 1991 [reapproved 1998].
[2] Polák J, Hájek M. Cyclic stress–strain curve evaluation using incremental step test procedure.Int J Fatigue May 1991;13:216–22 [May 1991].
[3] Polák J, Klesnil M, Lukáš P. On the cyclic stress–strain curve evaluation in low cycle fatigue. Mater Sci Eng April 1977;28:109–17.
[4] ASM Handbook (formerly Ninth Edition, Metals Handbook). Powder Metallurgy, vol. 7. USA: ASM International; 1984.
[5] ASM Handbook (formerly Tenth Edition, Metals Handbook). Properties and Selection: Nonferrous Alloys and Special-Purpose Materials, vol. 2. USA: ASM International; 1990.
[6] ASTM. Standard Test Methods for Tension Testing of Metallic Materials, E8; 2000.
[7] ASTM. Standard Practice for Conducting Force Controlled Constant Amplitude AxialFatigue Tests of Metallic Materials, E466; 1996.
[8] Lee YL, Pan J, Hathaway RB, Barkey ME. Fatigue testing and analysis. UK: Elsevier Butterworth Heinemann; 2005.
[9] Rao JNK, Subrahmaniam K, Owen DB. Effect of non-normality on tolerance limits which control percentages in both tails of normal distribution. Technometrics 1972;14:571–5.
[10] Owen DB. Variable acceptance sampling with non-normality. Technometrics 1969;11:631–7.
[11] Suresh S. Fatigue of materials. 2nd ed. Cambridge University; 1998.
[12] Ganesh Sundara Raman S, Padmanabhan KA. Determination of the room temperature cyclic stress–strain curve of AISI 304LN austenitic stainless steel by two different methods.Int J Fatigue September 1992;14:295–304 [September 1992].
[13] ASTM. Standard Practice for Strain-controlled Fatigue Testing, E606; 1992 [reapproved 1998].
[14] Chawla N, Murphy TF, Narasimhan KS, Koopman M, Chawla KK. Axial fatigue behavior of binder-treated versus diffusion alloyed powder metallurgy steels. Mater Sci Eng A 2001;308:180–8.
[15] Woodward RL, O'Donnell RG. Tensile rupture of tungsten alloys by cascade of crack nucleation events. J Mater Sci 2000;35:4067–72.
[16] Chawla N, Deng X. Microstructure and mechanical behavior of porous sintered Steels. Mater Sci Eng A 2005;390:98–112.
[17] Das J, Appa Rao G, Pabi SK. Microstructure and mechanical properties of tungsten heavy alloys. Mater Sci Eng A 2010;527:7841–7.
[18] Edmonds DV. Structure/property relationships in sintered heavy alloys. Int J Refract Met Hard Mater 1991;10:15–26.
[19] Ostolaza Zamora KM, Gil Sevillano J, Fuentes Pérez M. Fracture toughness of tungsten heavy metal alloys. Mater Sci Eng A 1992;157:151–60.
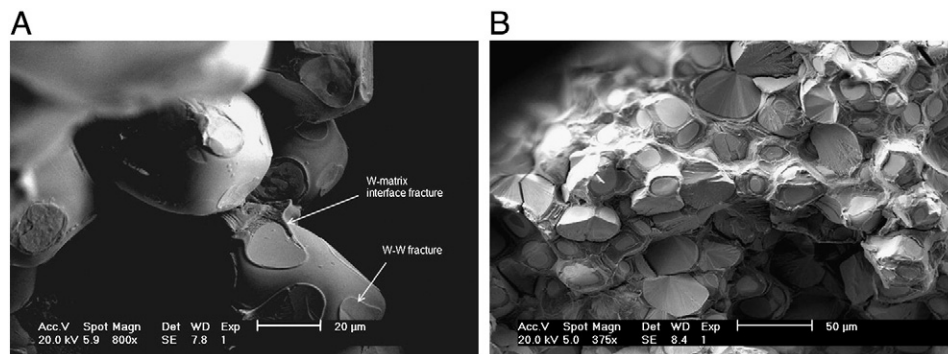
Fig. 17. Fracture surface of (A) IT180 and (B) D176 after stress-controlled fatigue fracture.